

Behic Mert  
Hartono Sumali  
Osvaldo H. Campanella

## A new method to determine viscosity of liquids using vibration principles

Received: 22 July 2002  
Accepted: 1 April 2003  
Published online: 22 July 2003  
© Springer-Verlag 2003

B. Mert · H. Sumali · O. H. Campanella (✉)  
Agricultural and Biological Engineering  
Department, Purdue University, West  
Lafayette, IN 47907, USA  
E-mail: camp@purdue.edu

**Abstract** A new method for determining viscosity of liquids is examined. The method employs the principles of vibration and measures the viscous damping due to the motion of a liquid placed in a cylindrical tube. The apparatus and the test liquid are treated as a dynamic system and the measured mechanical impedances are used to calculate energy dissipation due to the viscous damping. The newly designed apparatus is able to generate shear deformations in the liquid without using moving solid surfaces. A harmonic varying force with a frequency close to the resonance frequency of the system is applied

through a piston and the resulting velocities of the oscillations generated in the system are measured. Liquids with higher viscosities result in lower velocities due to the higher damping. Analytical equations are provided to relate the viscous damping of the dynamic system to the viscosity of the liquids. The viscosities obtained from the proposed method are in good agreement with the ones obtained from standard rotational viscometry using a cone and plate geometry.

**Keywords** Rheology · Viscosity · Viscous damping · Slip · Oscillation

### Introduction

Many rheological techniques do not take slip into account; however the results are often valid for industrial purposes because it can be argued that slip may also occur between solid surfaces and processed liquids in actual processing conditions. However, true rheological behavior of materials under shear can be obtained accurately only by eliminating the effect of slip and its effect on the shear flow. It has been recognized that two-phase or multiphase systems such as emulsions, foams, and complex biological liquids may violate the no-slip condition at solid boundaries, particularly when high shear stresses are applied. It is speculated that, for concentrated dispersions, this might be caused by the migration of the dispersed phase away from the solid surfaces, leaving a reduced concentration and low viscosity layer of liquid in contact with this surface

(Yoshimura and Prud'homme 1988). Another type of slip phenomena has been reported by Lim and Schowalter (1989), who showed that viscous liquids, such as for example polymer melts, may lose their adhesion to the wall and slide along it in slip-stick fashion, thus violating the no-slip assumption at the boundary between the testing fluid and the solid surface. These phenomena and the effects of slip on the rheological characterization of fluid systems have been reviewed by Barnes (1995). Most analyses and slip corrections in shear-based rheometry have been based on Mooney's approach (Mooney 1931), which assumes that the slip velocity at the solid surface is dependent on the shear stress. When this approach is applied to a small angle cone and plate system, which provides uniform shear rate and shear stress fields, one would expect that if slip is present it will produce the same slip in both the cone and the plate elements regardless of which one is the moving element of the

geometry. However, Britton and Callaghan (1997), using Nuclear Magnetic Resonance visualization in a cone and plate flow, showed that shear stress is not the sole determinant of slip velocity as assumed by Mooney's approach. Visualization of the flow in the cone and plate geometry showed that the magnitude of the velocity of the rotating cone could induce slip and that the higher the linear velocity of the fluid in contact with the moving cone, the larger the induced slip in the cone surface. This experimental realization is somewhat intuitive as it is expected that the chances of having slippage would increase with the velocity of the surface dragging the fluid. Moreover and as schematically shown in the article by Yoshimura and Prud'homme (1988), in which the same slippage is assumed in both plates of a parallel plate system, the elimination of slippage in one of the plates would contribute to reduce the error in the calculation of the true shear rate.

One way to minimize slippage at liquid and solid boundaries is by generating shear in the liquid without using a solid moving surface. The work discussed in this article utilizes that principle and introduces a new method to induce a shear flow without a solid moving surface. It differs from that used in conventional rotational steady shear or oscillatory tests in which a moving solid surface is utilized to induce the shear deformation and the no-slip condition is required to calculate the shear rate or shear strain applied to the sample. The principle of moving the test fluid to generate the shear flow is used in capillary viscometry; however in this method the viscosity is determined assuming a steady flow. Thurston (1969) developed a theory to describe the oscillation of a viscoelastic fluid in a circular tube using acoustical methods. The theory has been used to design a new viscometer able to determine viscoelastic properties of low viscosity liquids ([www.vilastic.com](http://www.vilastic.com)).

As schematically illustrated in Fig. 1, the proposed method oscillates part of the testing liquid itself to produce a harmonically varying shear deformation in the annular part of the flow domain. Although the induced shear deformation varies harmonically, measurements from the test are related to the viscous damping owing to

the liquid viscosity; thus only viscous properties of the liquid are determined with the proposed method. To highlight the advantage of the new method, Fig. 1 schematically illustrates momentary liquid velocities at the boundary between a moving solid surface and the testing liquid in a conventional shear-based rheological test (Fig. 1a) and at the hypothetical boundary between a moving "rigid body" liquid zone (P) and a shear deformed moving zone (S in Fig. 1b). In Fig. 1a the difference between the velocity of the solid surface and the liquid in contact with this surface, due to the presence of slip, is indicated as  $\Delta v_x$ . The non-slip condition requires that  $\Delta v_x = 0$ . Figure 1a also illustrates the potential problem that occurs when the liquid partially slips at the moving solid surface. The shear test relies on the assumption that the liquid at the solid-liquid interface moves at the same velocity as the solid surface. In reality, the velocity of the liquid at the interface may be less than the velocity of the solid surface ( $\Delta v_x > 0$ ) and this might result in erroneous calculations of the shear rate and thus the liquid viscosity. Although not indicated in the figure it is important to note that, according to Mooney's approach, slip should also occur at the stationary surface. The proposed method (Fig. 1b) works by inducing a known velocity in part of the liquid (region P). At the stationary liquid-solid interface, the velocity of the liquid layers largely diminishes due to viscous damping. Thus, slippage between the liquid and the stationary solid surface is expected to be very small, if it exists at all, as demonstrated in the recent study by Britton and Callaghan (1997). Conversely, slippage should be considered at the stationary surface if slippage exists at the moving boundary when the Mooney's approach is applied. The objective of this study was to design a method that reduces slippage either partially, when the Mooney's principle applies, or totally when the findings of Britton and Callaghan apply. In order to test the feasibility of the method, apparent viscosities of simple liquids were measured using the newly designed method and compared with those determined from standard shear-based rheometry.

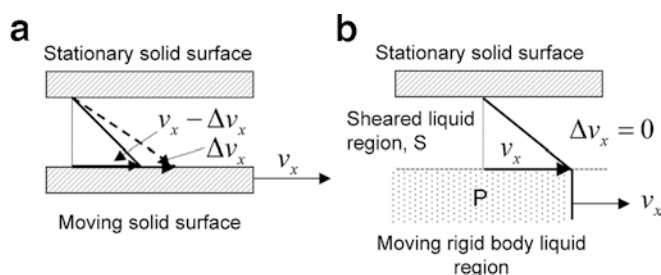


**Fig. 1a,b** Schematic of a simple shear deformation test and the presence of slip: **a** using standard shear test; **b** using the newly developed method

## Design and setup of the apparatus

The apparatus, shown schematically in Fig. 2, consisted of a stainless steel tube of 50 cm length and 3.8 cm internal diameter. Two circular pistons (3.68 cm in diameter) with springs attached to them were located at each end of the tube. The pistons were in contact with the liquid that fills the tube. To prevent liquid leakage, thin latex films were placed between the pistons and the liquid. A harmonic force applied to the driver piston (piston I) resulted in a vibration of the system composed of the pistons and the liquid contained between them. The frequency of oscillation of the driver piston dictates

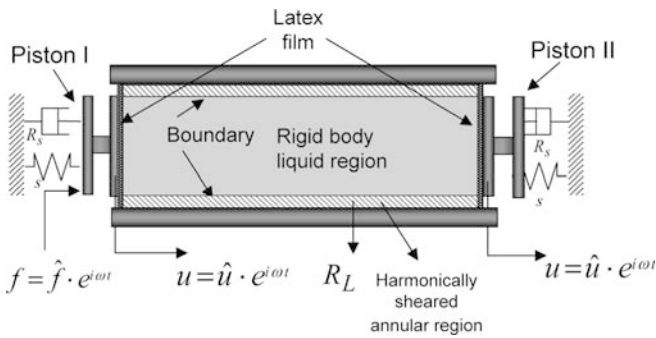


**Fig. 2** Schematic physical representation of the apparatus used in the research

the response of the system. If the wavelength ( $\lambda$ ) is much larger than the dimensions of the tube (both diameter and length), the pistons and the liquid between them vibrate as a rigid body in which the displacement is only a function of time. When the driver piston oscillates at frequencies such as the wavelength of the oscillation motion is comparable to the characteristic length of the tube, standing waves are generated in the liquid, and the liquid displacement depends on both time and position. The study presented in this paper focuses on the rigid body vibration phenomenon, that is when the driver piston is subjected to oscillations of low frequency and the driver piston, the liquid between the pistons and the receiver piston, all oscillate with the same frequency and in-phase.

During this “rigid body” liquid oscillation the geometry of the apparatus is similar to the Segel-Pochettino geometry (Ferry 1980), which is basically made of two coaxial cylinders and the test fluid is located in the annular region between them. Fluid in the annular region is sheared by applying a harmonic force on one of the cylinders and the resulting displacement in the other cylinder is measured. The newly designed instrument does not include the actual physical inner cylinder; instead a harmonically oscillating liquid inner region is created at the center of the tube by applying a harmonic force on the driver piston. Experimental results indicated that the flow created at the center of the tube is a cylindrical liquid region with a diameter equal to the diameter of the pistons. The evidence of this type of flow in piston driven flows has been demonstrated in a recent study by Lukner and Bonnecaze (1999) using a laser-sheet flow visualization technique.

As a consequence of the inner moving “rigid body” liquid flow there is a liquid interface that limits an un-sheared inner core region (shaded area) and a sheared annular region (patterned area) which are schematically illustrated in Fig. 2. If the two pistons and the liquid contained between them oscillate as a lumped element the liquid boundary between the sheared and un-sheared regions will oscillate with the same velocity than the

pistons and the annular region between this moving liquid boundary and the tube wall also oscillates harmonically. However, it will be shown that this oscillation lags the oscillation of the central core un-sheared liquid. A schematic of the flow fields induced by the system is shown in Fig. 3.

Oscillations in the annular sheared liquid layer can be considered as damped shear waves moving away from the moving liquid boundary in a direction perpendicular to the direction to the liquid oscillation. These shear waves decay due to the viscous forces until the velocity of the liquid is zero near the solid stationary boundary. A zone, known as penetration zone, which depends on the liquid properties, specifically viscosity and density, and the oscillation frequency was defined by Lamb (1945).

In order to measure the damping caused by the viscous forces the experimental setup schematically shown in Fig. 4, was designed. An actuator made of a

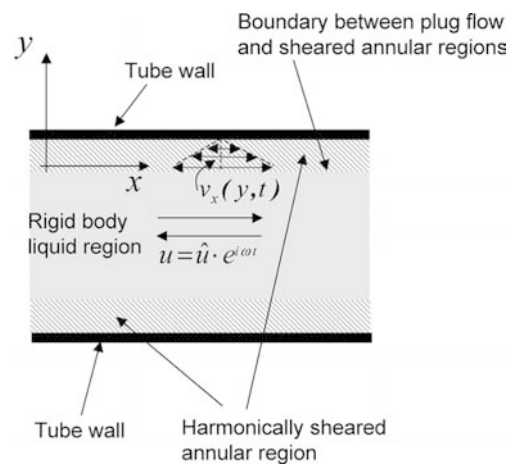


**Fig. 3** Geometry used for the theoretical analysis and schematic representation of the different flow regions in the tube

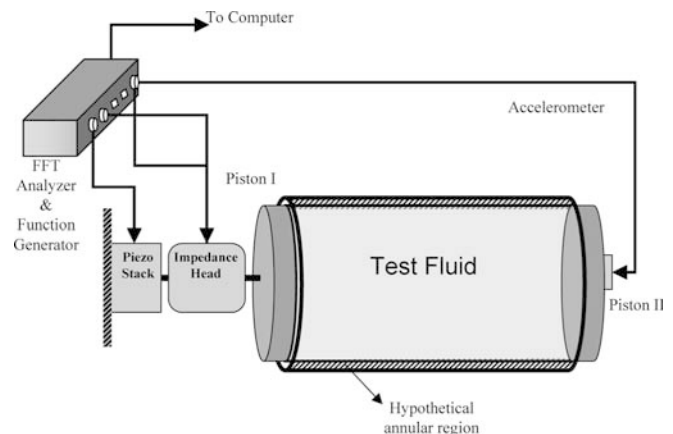


**Fig. 4** Experimental setup used in the research

stack of piezoelectric crystal layers was driven by a function generator and used as the force generator. The acceleration and force applied to the driver piston (piston I) were measured using an impedance head affixed to that piston. Similarly, the acceleration of the second piston (piston II) was measured using an accelerometer. Both the force and acceleration signals, acquired in the time domain of the experiment, were input into a Fast-Fourier-Transform (FFT) Model 2042 DSPT SigLab analyzer to obtain complex acceleration and force. This signal processor is capable of delivering measurements to a MATLAB environment. The measurements from the force transducer and accelerometer were averaged for eight trials per each liquid by the MATLAB VNA program and these averaged values were used in the calculations.

In order to validate the proposed method carboxyl-methyl-cellulose (CMC) solutions of different concentrations were used as test liquids. Their viscosities were determined using an ATS Viscotech Rheometer with a cone and plate geometry.

During the experiments two types of excitations were used. First, the frequency response of the system was determined for a wide range of frequencies (0–500 Hz) by exciting the system with random frequencies. This measurement enabled to determine the frequency range in which the system behaved as a lumped element. Second, forces at a single frequency were applied instead of random frequencies. The complex velocities of the pistons were measured to obtain the friction caused by the liquid in the annular sheared region.

## Theory

For frequencies at which the system behaves as a lumped element, the equation of motion for the force excited spring-mass-damper system, schematically described in Fig. 5, can be expressed as

$$f(t) = m\dot{u}(t) + Ru(t) + s \int u(t)dt \quad (1)$$

The symbols  $\dot{u}$ ,  $u$ , and  $\int u(t)dt$  denote acceleration, velocity, and displacement of the mass  $m$  respectively. The mass of the system is simply the sum of the masses of the pistons and the liquid contained between the

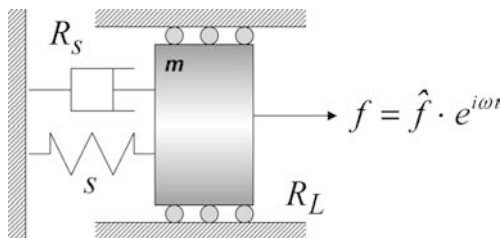


Fig. 5 Lumped model of the system

pistons. For a harmonic excitation it is more convenient to express the equation of motion in complex form. This can be achieved by applying the Fourier transform to Eq. (1) to give

$$\hat{f} \cdot e^{i\omega t} = i\omega m \hat{u} e^{i\omega t} + R \hat{u} e^{i\omega t} - \frac{is}{\omega} \hat{u} e^{i\omega t} \quad (2)$$

where  $\hat{f}$  and  $\hat{u}$  are the time independent phasors which contain amplitude and phase information and  $\hat{u}$  is the angular frequency. For test liquids with negligible elastic component, the springs which support the moving pistons are the only contributors to the stiffness  $s$ . Furthermore, the resistance to the fluid displacement ( $R$ ) is composed of two parts; the first is the damping of the piston-spring system denoted by  $R_S$  which can be determined from the frequency response function of the pistons alone. The other is related to the friction caused by the liquid at the annular sheared zone, and it is denoted by  $R_L$ . The sum of these resistances can be determined as

$$R_L + R_S = \Re(\hat{Z}) \quad (3)$$

where  $\hat{Z}$  is the complex impedance, defined as the ratio between the complex force and the complex velocity and  $\Re$  indicates the real part of the complex impedance. For the design used in this study  $R_L$  was much larger than  $R_S$ .

The viscous retarding force to the oscillatory motion can be obtained from the equation of motion. When the gap between the moving and the stationary surfaces is small and the viscosity is high, inertial effects can be neglected, and the viscous retarding force can be obtained without solving the equation of motion (Ferry 1980). However, when the oscillation amplitudes are large, the inertial effect ( $\rho \frac{Dv}{Dt}$ ) is no longer negligible (Ding et al. 1999). Thus, inertial effects have to be included in developing mathematical equations.

The general form of the equation of motion is

$$\rho \frac{Dv}{Dt} = -[\nabla \cdot \tau] - \nabla p + \rho g \quad (4)$$

where  $D$  indicates the Lagrangian derivative,  $v$  is the fluid velocity vector, and  $\tau$  is the stress tensor. The symbols  $p$ ,  $\rho$ , and  $g$  represent the pressure, density, and gravitational constant respectively. Neglecting the curvature of the annular region, which is appropriate for small gaps, the flow can be considered to be equal to that created in a simple shear test between two parallel plates whose kinematics is given by  $v_x = v_x(y, t)$ ,  $v_y = 0$ , and  $v_z = 0$ . Thus, the equation of motion for incompressible fluids in the coordinate system illustrated in Fig. 3 simplifies to

$$\rho \frac{\partial v_x}{\partial t} = \mu \frac{\partial^2 v_x}{\partial y^2} \quad (5)$$

where  $v_x$  is the velocity of the fluid in  $x$  direction and  $\mu$  is the viscosity of the fluid.

Since the liquid in the unshered liquid region and its boundary have a harmonic oscillatory motion they will induce the same harmonically varying velocity to the liquid located in the annular sheared region. Therefore, the time dependent complex velocity will be in the form of

$$\tilde{v}_x(y, t) = \hat{F}(y) \cdot e^{i\omega t} \quad (6)$$

Substitution of Eq. (6) into Eq. (5) yields

$$\hat{F}''(y) - iK^2\hat{F}(y) = 0 \quad (7)$$

where  $K^2 = \frac{\rho\omega}{\mu}$ .

Integration of Eq. (7) gives

$$\hat{F}(y) = \hat{A}e^{\left[\frac{K}{\sqrt{2}}(1+i)y\right]} + \hat{B}e^{\left[-\frac{K}{\sqrt{2}}(1+i)y\right]} \quad (8)$$

where  $\hat{A}$  and  $\hat{B}$  are complex constants; thus, the time independent complex velocity of the liquid is

$$\tilde{v}_x(y, t) = \left[ \hat{A}e^{\left[\frac{K}{\sqrt{2}}(1+i)y\right]} + \hat{B}e^{\left[-\frac{K}{\sqrt{2}}(1+i)y\right]} \right] e^{i\omega t} = \hat{v}_x(y)e^{i\omega t} \quad (9)$$

The boundary conditions  $\hat{v}_x(0) = \hat{u}$  and  $\hat{v}_x(h) = 0$ , i.e., non slip conditions, are used to estimate the constants  $\hat{A}$  and  $\hat{B}$  which yield the expression for the liquid velocity in the sheared layer of thickness  $h$  (Lamb 1945)

$$\hat{v}_x(y) = \hat{u} \frac{\sinh\left[(1+i)\frac{K}{\sqrt{2}}(h-y)\right]}{\sinh\left[(1+i)\frac{K}{\sqrt{2}}h\right]} \quad (10)$$

The viscous retarding force per unit area that causes the damping of the oscillatory motion can be obtained from the shear stress at the boundary between the plug flow and the annular sheared regions, that is

$$(\tilde{\sigma}_{xy})_{y=0} = -\mu \left( \frac{\partial \tilde{v}_x}{\partial y} \right)_{y=0} e^{i\omega t} \quad (11)$$

where  $\tilde{\sigma}_{xy}$  indicates complex shear stress. Substitution of Eq. (10) into Eq. (11) yields

$$(\tilde{\sigma}_{xy})_{y=0} = \hat{u}\mu(1+i)\frac{K}{\sqrt{2}}\coth\left((1+i)\frac{K}{\sqrt{2}}h\right)e^{i\omega t} \quad (12)$$

The velocity of the piston and thereby the velocity of the liquid in the plug flow region can be obtained as the real part of the complex velocity with a certain phase angle  $\Phi$ , that is:

$$u = \Re\left(U_0e^{i(\omega t + \phi)}\right) = \Re(\hat{u}e^{i\omega t}) \quad (13)$$

Therefore the actual viscous retarding force per unit area can be calculated as the real part of the expression given by Eq. (12), which is obtained using the software Mathematica, as

$$(\sigma_{xy})_{y=0} = \frac{KU_0\mu[\sin(\sqrt{2}Kh)(\cos(\omega t + \phi) + \sin(\omega t + \phi)) - \sinh(\sqrt{2}Kh)(\cos(\omega t + \phi) - \sin(\omega t + \phi))]}{\sqrt{2}(\cosh(\sqrt{2}Kh) - \cos(\sqrt{2}Kh))} \quad (14)$$

Practically, during the oscillatory motion, the system performs work against the friction forces at a certain rate that depends on the liquid viscosity. The power dissipation per unit surface area can be obtained as

$$\dot{W}_{\text{friction}} = -(\sigma_{xy})_{y=0}v_x(0, t) \quad (15)$$

This dissipation can also be expressed in terms of experimentally measured variables as

$$\dot{W}_{\text{friction}} = \Re\left(\frac{R_L U^2}{A}\right) = \frac{R_L U_0^2}{A}\cos^2(\omega t + \phi) \quad (16)$$

Equations (15) and (16) represent momentary dissipation by friction of the system at a given time. In order to obtain the friction over a period of time, a time-averaged form of the above expressions can be used. Considering the time average and equating integrated forms of Eqs. (15) and (16) along with Eqs. (9), (10), and (14) yields the following equation:

$$\begin{aligned} & \frac{1}{T} \int_0^T \frac{R_L U_0^2}{A} (\cos^2(\omega t + \phi)) dt \\ &= \frac{1}{T} \int_0^T \frac{KU_0^2\mu\cos(\omega t + \phi) [\sin(\sqrt{2}Kh)(\cos(\omega t + \phi) + \sin(\omega t + \phi)) - \sinh(\sqrt{2}Kh)(\cos(\omega t + \phi) - \sin(\omega t + \phi))]}{\sqrt{2}(\cosh(\sqrt{2}Kh) - \cos(\sqrt{2}Kh))} dt \end{aligned} \quad (17)$$

from which the following expression can be obtained:

$$\mu \left[ \frac{\sin\left(h\sqrt{\frac{2\rho\omega}{\mu}}\right) + \sinh\left(h\sqrt{\frac{2\rho\omega}{\mu}}\right)}{\cos\left(h\sqrt{\frac{2\rho\omega}{\mu}}\right) - \cosh\left(h\sqrt{\frac{2\rho\omega}{\mu}}\right)} \right]^2 = 2 \frac{R_L^2}{A^2} \frac{1}{\rho\omega} \quad (18)$$

Equation (18) gives a relationship between the geometrical parameters of the system, the properties of the liquid, the frequency of the oscillations, and the measured resistance owing to the friction, denoted by  $R_L$ . The solution of this equation can be obtained numerically and results are illustrated in Fig. 6 for the geometrical parameters used in this study. It shows the existing relationship between the viscosity of the liquid and the damping due to the liquid friction  $R_L$ . Figure 6 clearly shows that if  $R_L$  is known it allows a quick estimation of the liquid viscosity either reading the value from the figure or by calculation through Eq. (18). As discussed,  $R_L$  can be obtained by measuring the complex impedance of the system  $\hat{Z}$  (see Eq. 3).

The experimental setup can be modified for the analysis of fluids with elastic characteristics because the working principle is similar to the apparatuses designed by Birnboim and Chompff (Ferry 1980; Schrag 1977). However, for the analysis of viscoelastic materials, instrument parameters such as spring stiffness and gap thickness must be set up according to the properties of material to be tested. For instance, the spring stiffness  $s$  must be comparable to the material elasticity to avoid loss of precision. Working equations for viscoelastic materials can be obtained by replacing the real, frequency independent, viscosity with the complex viscosity  $\eta^* = \eta' - i\eta''$ . The solution of the diffusion equation

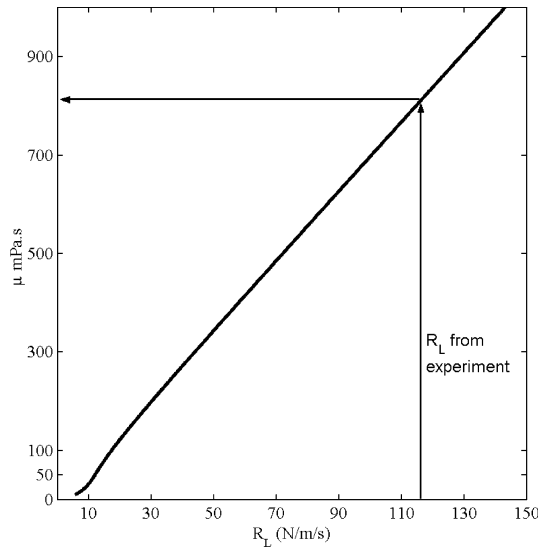


**Fig. 6** Plot of liquid viscosity as a function of the experimentally obtained  $R_L$

(Eq. 5), including the complex viscosity, that satisfies the non-slip boundary conditions is

$$\hat{v}_x(y) = \hat{u} \frac{\sinh\left[(i\rho\omega/\eta^*)^{0.5}(h-y)\right]}{\sinh\left[(i\rho\omega/\eta^*)^{0.5}h\right]} \quad (19)$$

and the shear field in the gap can be obtained as

$$\dot{\gamma} = -\hat{u}[i\rho\omega/\eta^*]^{0.5} \frac{\cosh\left[(i\rho\omega/\eta^*)^{0.5}(h-y)\right]}{\sinh\left[(i\rho\omega/\eta^*)^{0.5}h\right]} \quad (20)$$

Equation (20) reduces to the equation of a shear field ( $\dot{\gamma} = -\hat{u}/h$ ) for a simple shear system if the quantity  $(i\rho\omega/\eta^*)^{0.5}$  is small compared to unity. This condition (negligible fluid inertia) is usually referred as “gap-loading” (Schrag 1977). Under gap-loading conditions the well known relations between complex mechanical impedance and material properties are given in Ferry (1980):

$$\eta''_{\text{gap-loading}} = \left[-\text{Im}(\hat{Z}) + \omega m - \frac{s}{\omega}\right] h/A \quad (21)$$

where  $\text{Im}(\hat{Z})$  is the imaginary part of the measured complex impedance.

The real component of the complex viscosity  $\eta'$  can be calculated as

$$\eta'_{\text{gap-loading}} = \text{Re}(\hat{Z}) h/A \quad (22)$$

However, under the influence of inertial effects Eqs. (21) and (22) are no longer valid. When inertial effects are significant a relationship between the true complex viscosity ( $\eta^*$ ) and the gap-loading complex viscosity can be obtained as (Böhme and Stenger 1989)

$$\eta^*_{\text{gap-loading}} = \eta^* h [i\rho\omega/\eta^*]^{0.5} \coth\left[(i\rho\omega/\eta^*)^{0.5}h\right] \quad (23)$$

Once  $\eta^*_{\text{gap-loading}} = \eta'_{\text{gap-loading}} - i\eta''_{\text{gap-loading}}$  is determined from Eqs. (21) and (22), Eq. (23) can be solved for  $\eta^*$ . Solution approximations and methodologies are described in Böhme and Stenger (1989).

## Results

Through the use of the DSP FFT analyzer frequency response functions were obtained for both random excitation frequencies and a single frequency of 33 Hz. This particular frequency was used because at frequencies higher than the resonance frequency of the system the inertia term, i.e., the term  $i(\omega m \dot{u} e^{i\omega t})$  in Eq. (2) becomes too large and decreases the precision of the measurement. If the system is excited at the resonance frequency, the response becomes too sensitive. Moreover, continuous excitation of the system at the resonance frequency would be very difficult to analyze

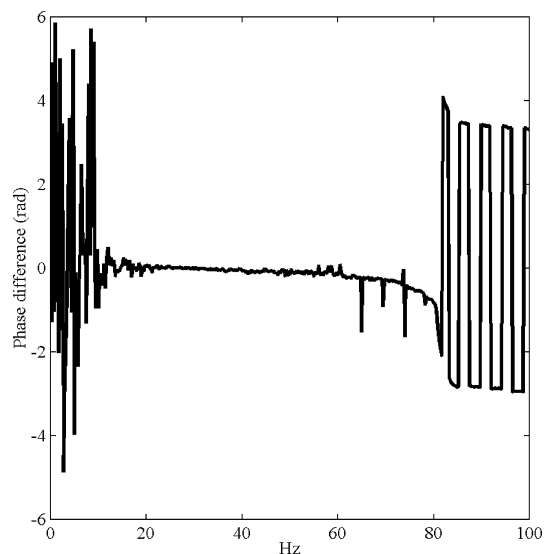


Fig. 7 Phase difference between pistons II and I

because significantly amplified responses might cause nonlinearities.

Figure 7 depicts the phase difference between velocities of the pistons I and II when the tube was filled with one of the CMC solutions and excited with random frequencies. The figure clearly shows that at frequencies below 60 Hz both piston velocities had the same phase angle. Although some phase differences appear below 20 Hz, this was mainly due to the lower sensitivity of the signal acquisition system at those low frequencies. Figure 8 shows measured velocity amplitude of pistons I and II. As illustrated, these amplitudes are almost identical

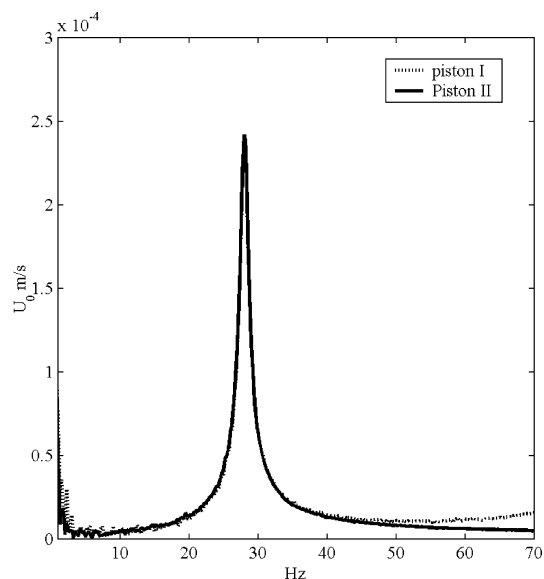


Fig. 8 Magnitude of piston velocities

for frequencies below 55 Hz. Thus, these results are indicating that both pistons have velocities with the same amplitude and are in phase. Since only piston I is driven by the force generator, it can be inferred that the liquid volume contained between the pistons must have the same velocity as the pistons, thus moving as a harmonic oscillating moving rigid body liquid region. The diameter of this region (unsheared liquid) must be equal to the diameter of the pistons otherwise the pistons would not have the same velocity. An important characteristic indicated in Fig. 7 is the formation of waves above 80 Hz. When standing or propagating waves are generated, the system is no longer lumped; in other words, it becomes a distributed system and viscous dissipation mechanism has to be analyzed in a completely different way. The analysis considered in this work only focuses on the lumped system. The formation of standing waves and determination of the liquid viscosity under these conditions are currently under investigation.

In order to validate the proposed method standard solutions were prepared by using various concentrations of CMC and their viscosities were measured in a rotational viscometer using a cone and plate geometry. As illustrated in Fig. 9 these solutions (indicated as CMC1, CMC2, and CMC3) exhibited Newtonian behavior for shear rates below  $10 \text{ s}^{-1}$ .

The force generator piezo crystals stack and the DSP function generator were used to excite the system at 33 Hz with a force of 0.55 N and the resulting velocities of the pistons were measured. Results are illustrated in Fig. 10. As indicated in the figure the solution with higher viscosity produced a larger damping; therefore, it had a lower velocity. From the real part of the complex ratio between force and velocity (Eq. 3) the resistances,  $R_L$ , for each of the samples were obtained. These values were used to calculate the sample viscosity from Eq. (18). As discussed the determination of the viscosity can also be done graphically. An example of graphic calculation of the viscosity for the sample CMC 3 is shown in Fig. 6.

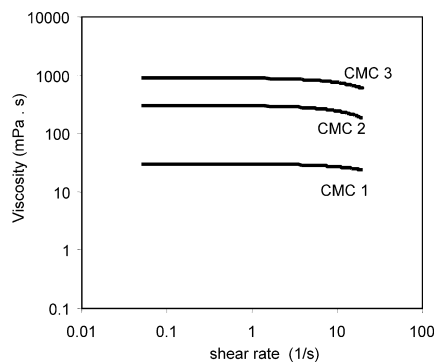
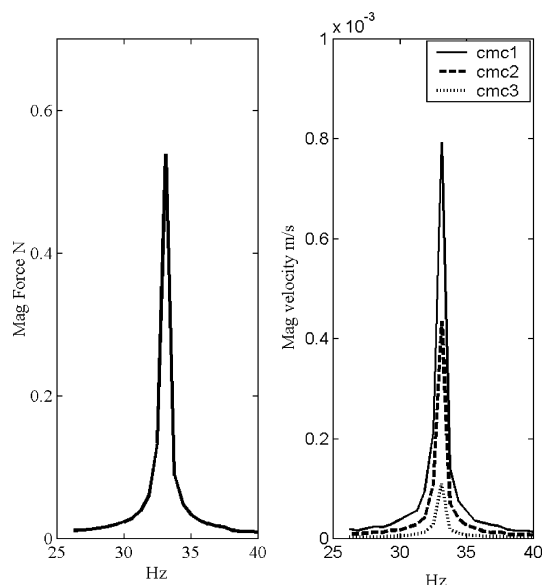


Fig. 9 Viscosity of the CMC solutions determined using rotational viscometer and cone and plate geometry

Since liquid samples may exhibit shear thinning behavior at relatively higher shear rates a comparison between results obtained with the proposed method and those obtained in standard viscometer can be done only if the shear rates of the two methods are similar. Furthermore, when the viscosity is high or the gap ( $h$ ) is small the effect of liquid inertia can be neglected as it is commonly done in standard oscillatory rheometry. When the liquid inertia is neglected the shear rate at  $y=0$  can be



**Fig. 10** Magnitude of the applied force and corresponding velocities

approximated to the ratio between the piston velocity and the gap thickness ( $h$ ). However, for low viscosity liquids deviations from the simple shear test may take place; consequently the shear rate cannot be calculated as the ratio of the piston velocity to the gap thickness. In order to show the effect of inertia on the estimation of the applied shear rate, the velocity profiles of liquids with different viscosities are shown in Figs. 11 and 12 for different times. In Fig. 11 the normalized velocity profile in the annular region for the liquid with a viscosity of 30 mPa.s is plotted at various times during one cycle.  $U_0$  denotes the measured velocity amplitude for this liquid. Since the viscosity was low and the designed gap thickness was not small enough, the effect of the liquid inertia can be observed in the deviation of the velocity profiles from linearity. Less pronounced inertia effects for the higher viscosity liquid (900 mPa.s) can be seen in Fig. 12 at all times in which velocity profiles during one cycle are nearly continually linear and the estimation of the shear rate as the piston velocity divided by the gap thickness can be used without appreciable error.

In this work the shear rate applied during the test is calculated using a more rigorous approach. That is, the shear rate at  $y=0$  is calculated by taking the derivative of the velocity profile in the sheared annulus (Eq. 10) with respect to the direction  $y$ . As illustrated in Fig. 13, in which the shear rate at  $y=0$  is plotted as a function of time, the liquid with the lowest viscosity had the shear rate with the largest amplitude. The highest shear rate for the 30 mPa.s CMC solution was calculated as  $2.6 \text{ s}^{-1}$ . As illustrated in the figure the amplitude of the shear rate decreased with increasing viscosity. Thus,

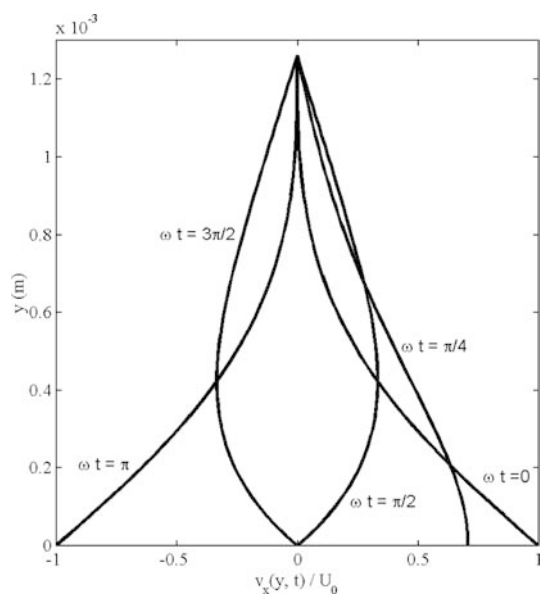


**Fig. 11** Velocity profile during one cycle for a fluid with viscosity 30 mPas

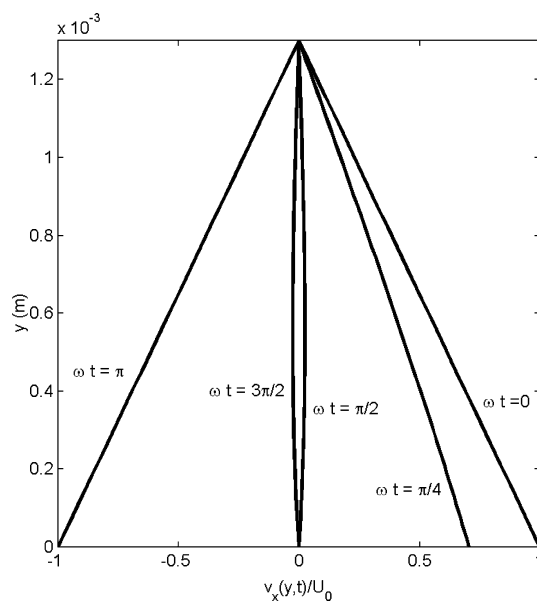


**Fig. 12** Velocity profile during one cycle for a fluid with viscosity 900 mPas

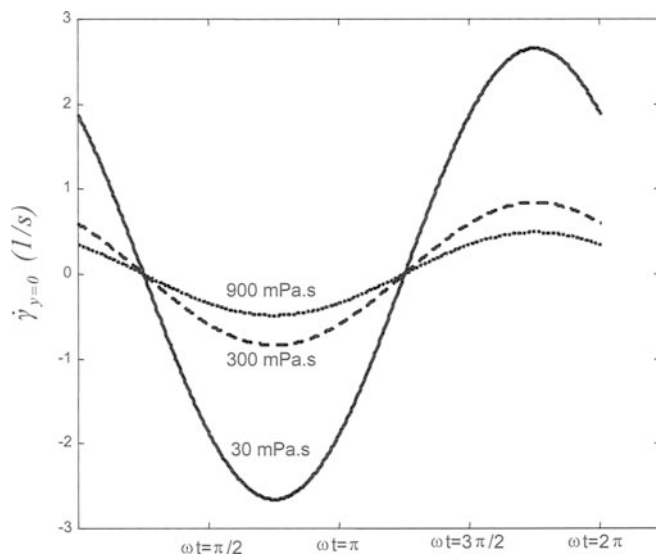


Fig. 13 Applied shear rates to samples with different viscosity

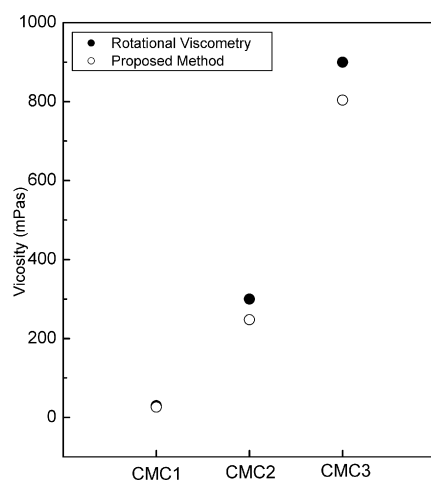


Fig. 14 Comparison of viscosities of CMC solutions measured with standard rheology and the newly developed method

the applied shear rates were within the range in which the tested liquids were Newtonian and the assumption of Newtonian behavior implicit in the derivation of Eq. (18) is satisfied. Figure 14 provides a comparison between viscosities of the three CMC solutions measured by the cone and plate geometry and the proposed method. As indicated in the figure viscosities obtained from both methods are in good agreement.

Current design of the instrument can be improved to meet specific requirements. First, by modifying the piston diameter the gap thickness can be optimized to eliminate computational requirements for the case that non-negligible liquid inertia has to be included in the calculations. Second, the resonance frequency of

the system is equal to the square root of the ratio of the spring stiffness to the mass ( $f_{\text{resonance}} = \sqrt{\frac{s}{m}}$ ). Thus decreasing the mass of the system or using a stiffer spring increases the resonance frequency at which the solid rigid mode may be used. This would allow the analysis at higher frequencies and, thereby, at higher shear rates. It is also possible to manufacture a highly miniaturized version of the instrument with low spring stiffness by which storage modulus ( $s$  in Eq. 2) of viscoelastic materials can be measured. Finally, the frequency of the oscillation can be increased to generate one-dimensional standing waves in the liquid and the measurement of the impedance at pistons I and II would make possible the measurement of the acoustic wave attenuation due to viscosity.

## Conclusions

In this study CMC solutions were used as standard solutions to show that viscosity values obtained from the well established cone and plate technique and the proposed method are in good agreement. CMC solutions were purposely used because there are no reported significant slip effects when testing these solutions using standard shear-based methods.

The liquid contained in a cylindrical tube is separated in two regions, an oscillatory moving rigid body liquid region in the center and a sheared annular region between that inner core region and the tube wall, both subjected to harmonic oscillation as the system is excited by a harmonic vibration of a given frequency. It was demonstrated that viscous forces in this annular sheared region can be measured with reasonable accuracy and within a wide range of values without using a solid moving surface to generate the shear deformation as done in standard shear based techniques.

Since the viscous penetration depth for the CMC solutions was larger than the gap between the liquid-liquid boundary and the stationary tube surface, measurement was still based on the no-slip assumption at the stationary tube wall. Furthermore, assuming a non-slip boundary condition at a stationary surface is intuitively more reasonable than assuming it at a moving surface. There is experimental evidence (Britton and Callaghan 1997) that suggests that slip is more favored in moving solid surfaces.

Slight modifications in the design of the apparatus should improve the range of shear rates which can be obtained by this instrument. Moreover miniaturized tube dimensions and softer springs can allow the study of viscoelastic properties of the materials. Future studies will involve the study of materials such as mayonnaise because it is well known that mayonnaise exhibits a great deal of slip when tested under shear deformations

(Plucinski et al. 1998; Goshawk and Binding 1998). Future studies will also involve the generation of standing waves with higher excitation frequencies in the tube than those used in this study in order to allow the analysis of standing wave attenuation due to viscous effects.

---

## References

- Barnes HA (1995) A review of the slip (wall depletion) of polymer-solutions, emulsions and particle suspensions in viscometers—its cause, character and cure. *J Non-Newtonian Fluid Mech* 56:221–251
- Böhme G, Stenger M (1989) On influence of fluid inertia in oscillatory rheometry. *J Rheol* 34(3):415–424
- Britton M, Callaghan PT (1997) Nuclear magnetic resonance visualization of anomalous flow in cone-and-plate geometry. *J Rheol* 41:1365–1386
- Ding F, Giacomin AJ, Bird RB, Kweon CB (1999) Viscous dissipation with fluid inertia in oscillatory shear flow. *J Non-Newtonian Fluid Mech* 86:359–374
- Ferry JD (1980) *Viscoelastic properties of polymers*. Wiley, New York, NY
- Goshawk JA, Binding DM (1998) Rheological phenomena occurring during shearing flow of mayonnaise. *J Rheol* 42:1537–1553
- Lamb H (1945) *Hydrodynamics*. Dover Publications, New York, NY
- Lim FJ, Schowalter WR (1989) Wall slip of narrow molecular weight distribution polybutadienes. *J Rheol* 33:1359–1382
- Lukner RB, Bonnecaze RT (1999) Piston-driven flow of highly concentrated suspensions. *J Rheol* 43:735–751
- Mooney M (1931) Explicit formulas for slip fluidity. *J Rheol* 2:210–222
- Plucinski J, Gupta RK, Chakrabarti S (1998) Wall slip of mayonnaises in viscometers. *Rheol Acta* 37:256–269
- Schrag JL (1977) Deviation of velocity gradient profiles from the 'gap loading' and 'surface loading' limits in dynamic simple shear experiments. *J Rheol* 21(3):399–413
- Thurston GB (1969) Theory of oscillation of a viscoelastic fluid in a circular tube. *J Acoust Soc Am* 32(2):210–213
- Yoshimura A, Prud'homme RK (1988) Wall slip corrections for couette and parallel disk viscometers. *J Rheol* 32:53–67